Evolution of the Properties of Al_nN_n Clusters with Size

Aurora Costales,*,† M. A. Blanco,† E. Francisco,† Ravindra Pandey,‡ and A. Martín Pendás†

Departamento de Química Física y Analítica, Facultad de Química, Universidad de Oviedo, 33006-Oviedo, Spain, Department of Physics, Michigan Technological University, Houghton, Michigan 49931

Received: September 9, 2005; In Final Form: November 2, 2005

A global optimization of stoichiometric $(AlN)_n$ clusters ($n = 1-25$, 30, 35, ..., 95, 100) has been performed using the basin-hopping (BH) method and describing the interactions with simple and yet realistic interatomic potentials. The results for the smaller isomers agree with those of previous electronic structure calculations, thus validating the present scheme. The lowest-energy isomers found can be classified in three different categories according to their structural motifs: (i) small clusters ($n = 2-5$), with planar ring structures and 2-fold coordination, (ii) medium clusters ($n = 6-40$), where a competition between stacked rings and globular-like empty cages exists, and (iii) large clusters ($n > 40$), large enough to mix different elements of the previous stage. All the atoms in small and medium-sized clusters are in the surface, while large clusters start to display interior atoms. Large clusters display a competition between tetrahedral and octahedral-like features: the former lead to a lower energy interior in the cluster, while the latter allow for surface terminations with a lower energy. All of the properties studied present different regimes according to the above classification. It is of particular interest that the local properties of the interior atoms do converge to the bulk limit. The isomers with $n = 6$ and 12 are specially stable with respect to the gain or loss of AlN molecules.

I. Introduction

The onset of crystalline behavior during cluster growth is one of the frequently asked questions within nanoscience. However, as pointed out by Martin,[1] this is an ill-posed question since different properties have different transition sizes into the bulk behavior. Hence, it is more meaningful to analyze the evolution of different properties, critically comparing them with their bulk counterparts. Our main aim in this article is to conduct such a study for $(AlN)_n$ stoichiometric clusters of increasing size. For this purpose, a global optimization (GO) that seeks the lowest-energy structure for a given size is needed. This is a very time-consuming task that requires thousands of local minimizations, each of them potentially requiring tens of cluster energy (and its derivatives) evaluations. Thus, a simple enough energy model that represents the essential features of the potential energy surface (PES) of the system is needed. In the present article, the interactions among the diffrent atoms in the cluster will be represented by means of interatomic pair potentials. Although this model is obviously less accurate than the current state-of-the-art electronic structure methods, it allows a more exhaustive exploration of the PES. On the other hand, this work continues a well-established line of research,[2−8] in which we have performed restricted GOs of small size stoichiometric clusters using ab initio methods. Thus, the present results can be both (i) tested against the known electronic structure results and (ii) used to restrict a further structural search of larger-sized isomers employing the same electronic structure methods as in the smaller clusters.

The reasons behind this research line are 2-fold. On one hand, group III nitrides are well-known as technologically important materials,[9−15] both in bulk and in thin film (epitaxially deposited)[16,17] forms. However, their application in the fabrication of nanostructures and nanodevices is only now beginning, and it is considered to have promising applications. On the other hand, the global optimization of nanostructures is still an open basic research problem (see the website: http://www-wales.ch.cam.ac.uk/CCD.html). Some progress has been made within homoatomic clusters: global minima for Lennard-Jones clusters (a model for rare-gas clustering) are known for a wide range of sizes,[18−23] also for quantum Lennard-Jones clusters,[24] and some work has been done with metal clusters (although not so systematic),[23−27] molecular clusters,[28,29] and other materials[30−32] (e.g., silicon). Among binary compounds, only the ionic alkali halide clusters have been studied with some depth[33] and, recently, Doye et al have studied binary Lennard-Jones clusters.[34] Thus, the interesting realm of partially ionic (or partially covalent) compounds is yet unexplored, although it will certainly provide results different both to the homoatomic cases (with symmetric bonds) and to the ionic compounds (where a large charge transfer occurs).

The paper is organized as follows. In the next section, we describe the pair potential model employed and how it has been obtained. In section 3, we present the global optimization method used in the generation of the most stable isomers. Section 4 presents our results, that is, the evolution of different cluster properties when increasing the cluster size. Finally, we will present our conclusions in the last section.

II. Pair Potentials

To describe the energy surface for the global optimization, we will use an atomistic pair potential model. Since we seek to understand the evolution of the properties of the clusters toward their bulk values, we will obtain the pair potentials within the solid-state context. The experimental structure of AlN is the hexagonal B4 structure with tetrahedral coordination. In our previous work,[6] we have used the more symmetric cubic B3

* To whom correspondence should be addressed. E-mail: yoyi@carbono.quimica.uniovi.es.

† Universidad de Oviedo.

‡ Michigan Technological University.

10.1021/jp055094j CCC: $33.50
Published on Web 00/00/0000 PAGE EST: 8.7

TABLE 1: Ab Initio Perturbed Ion Short-Range Potential Parameters for the Different Interactions in the AlN Systems[a]

pair $i-j$	A_1^{ij}	n_1^{ij}	ρ_1^{ij}	A_2^{ij}	n_2^{ij}	ρ_2^{ij}
Al−N	100.458816	0	2.182429			
Al−Al	−41.557010	0	1.171765	60.196250	−1	0.924620
N−N	84.586517	1	2.042760	−151.886016	3	2.995922

[a] All constants are in atomic units.

structure, also tetrahedral, which is attainable in the metastable phase by epitaxial deposition. We selected a B3 configuration equivalent to the experimental B4 one by equating its volumes per formula unit, so that the B3 nearest-neighbor distance becomes 1.888 Å (3.568 a_0). For this structure, we did obtain atomic charges within the quantum theory of atoms in molecules (QTAM),[35] being −2.39 e for N (compare, e.g., with −1.88 as computed by Xu and Ching[36]). This value indicates that the solid has a significant ionic character. Previous ab initio calculations[7,8] have shown that the $(AlN)_n$ ($n = 1, 6$) clusters have a very polar bond with a high ionic character, with their QTAM atomic charge values for N ranging from −0.94 e in the molecule to −2.24 e in the hexamer. Consequently, we expect that a good qualitative description of these clusters can be achieved with only the consideration of the long-range Coulombic potential plus a short-range two-body interaction. A quite general, analytic expression for this is

$$V_{ij}(r) = \frac{q_i q_j}{r} + \sum_m A_m^{ij} r^{n_m{}^{ij}} \exp(-\rho_m^{ij} r) \qquad (1)$$

To obtain crystal-adapted interatomic potentials, we have used in-solid ab initio pertubed ion[37] (ai PI) atomic descriptions to compute each interatomic potential at a range of distances.[38,39] We have restricted ourselves to the so-called *rigid* potentials, meaning that when using these potentials a single atomic description is used to obtain the potential for every distance. After a wide and careful analysis, and considering the atomic charges exhibited by the crystal and the small clusters, we have chosen a partial ionic description for the AlN crystal at the experimental geometry, which uses net ionic charges of +2 e and −2 e for Al and N, respectively. This description is used both for the long-range Coulombic term and for the ionic wave functions used in this model to generate the short-range potential. The resulting ab initio perturbed ion short-range potentials are fitted to the last term in eq 1, giving the parameters presented in Table 1. Several other schemes have also been tested, which include (i) using the electron gas model by Gordon and Kim[40−43] to generate the short-range interaction, (ii) using nominal ionic charges for the Coulombic interaction and/or the ionic wave functions, and (iii) introducing a charge-transfer model depending on the interatomic distances. However, the selected potential model gave the best results both for the crystal and for the small clusters (as compared to previous DFT calculations, see refs 6,7, and 8 and references therein), presenting a good balance between the different interactions.

III. Isomers Generation

The main problem in the study of the cluster properties and their convergence to the bulk limit lies in the need to exhaustively explore the potential energy surface (PES) to locate the global minimum (GM) or lowest-energy structure. Since the number of stable isomers increases exponentially with cluster size, except for small clusters (≃2−20 atoms), thousands of local minimizations are required before one has the relative assurance that the GM has been found. This increase stresses also the problem of numerically distinguishing those local minima which are truly different since, very frequently, an achieved geometrical configuration may in fact be equivalent to a previous one after a suitable rotation of the coordinates. To perform the local minimizations and the analysis of the different isomers, we have used our own *cluster* code.[44] This is an atomistic program that allows us to generate thousands of isomers or stable configurations of a given molecular complex by means of advanced optimization techniques. In this code, the interactions among the different atoms in the cluster can be described by means of several types of interatomic potentials, including those described in section 2.

Different algorithms have been developed over the years to locate the GM of a cluster.[45] In this article, we have carried out all the global minimizations employing the basin-hopping (BH) method developed by Wales, Doye, and Scheraga.[18,46] This has shown to be an unbiased and robust technique able to deal successfully with Lennard-Jones,[18] alkali halides,[33] aromatic hydrocarbons,[47] silicon,[48] or metallic clusters.[26] The basic idea of the basin-hopping method is to perform a Monte Carlo minimization of the transformed PES defined by $\bar{E}(\mathbf{X}) = \min\{E(\mathbf{X})\}$, where $\mathbf{X}$ represents the vector of nuclear coordinates. In this way, the transformed energy at $\mathbf{X}$ is assigned to that of the local minimum obtained by an optimization starting from that point. The atomic positions at each Monte Carlo step, $\mathbf{X}_{old}$, are randomly displaced by a number in the range [−1, 1] times a prefixed maximum value. The new atomic positions, $\mathbf{X}_{new}$, are accepted if $\bar{E}(\mathbf{X}_{new}) \leq \bar{E}(\mathbf{X}_{old})$ or $\exp\{[\bar{E}(\mathbf{X}_{old}) - \bar{E}(\mathbf{X}_{new})]/kT\} > r$, where r is a random number drawn from the interval [0,1]. In this work, the maximum random displacement was adjusted to give an acceptance ratio of 50%. We have implemented the BH technique in the *cluster* code based on the freely available routines of the *Gmin* program by Wales (http://www-wales.ch.cam.ac.uk/software.html). The *cluster* program also performs most of the analyses that will be presented in the following sections. The geometry optimization method employed here to minimize each new structural configuration provided by the BH method is the limited-memory BFGS (Broyden, Fletcher, Goldfarb, and Shanno) variant of the DFP (Davidson, Fletcher, and Powell) method, as implemented by Nocedal and Liu[49] for performing large scale optimizations. We have employed the following convergence criteria: 10^{-10} E_h for the energy, 10^{-7} a_0 for the coordinates, and 10^{-6} E_h/a_0 for the modulus of the gradient. The starting configurations of the BH runs were generated by randomly placing the atoms in a cubic box whose edge increases linearly with the cluster size ($n = 1-10$) or by means of a previous global minimization using the algorithm of Phillips et al.[50] ($n = 11-100$). After these initial configuration generations, the BH algorithm is applied. A BH global minimization run with 3000, 6000, 10 000, 20 000, 25 000, and 50 000 Monte Carlo steps has been employed for $1 \leq n \leq 5$, $6 \leq n \leq 10$, $11 \leq n \leq 15$, $16 \leq n \leq 20$, $21 \leq n \leq 25$, and $30 \leq n \leq 50$, respectively, giving us a good degree of confidence in the obtained minima. For the clusters with $n > 50$, we employed three consecutive BH global minimizations runs with 15 000 Monte Carlo steps each.

After several local minima (and, presumably, the GM) on the PES have been found for a given size, it is not always trivial to discriminate which of them correspond to really different isomers. In clusters formed by few atoms, a visual inspection can suffice to establish whether two structures are identical or not. However, in more complex systems, quantitative and automatic criteria are needed. In the *cluster* code, several of

these criteria are available, and we have chosen to apply them in a cascade fashion. First, the full set of optimized clusters is analyzed according to the molecular graph criterion (see ref 51 for details), giving a number of smaller subsets. Now, the energetic criterion (two clusters are different if the relative energy difference is bigger than a quantity, 10^{-6} E_h in this case) is applied to the clusters of every subset, giving place to new, refined subsets. Finally, the inertia moment criterion (two clusters are considered different if the relative difference between any of their three principal inertia moments is bigger than a quantity, 10^{-2} $m_e a_0^2$ here) is applied to each subset, splitting them into a final group of subsets, each of them being ascribed to a single isomer. The reduced final list of different isomers after the above procedure is submitted to another reoptimization process, which can now be more strict. For this purpose, we have employed an eigenvector following algorithm[45] with the following convergence criteria: 10^{-12} E_h for the energy, 10^{-10} a_0 for the Cartesian coordinates, and 10^{-8} E_h/a_0 for the modulus of the gradient. To verify whether any critical point obtained in the minimizations is actually a minimum of the PES, a vibrational analysis was performed at that point. No imaginary frequencies were found in any case.

The calculations have been performed on a Pentium IV computer running GNU/Linux. The CPU time (t) required for these optimization + analysis runs depends on the cluster size and the initial configuration generation strategy, as described above. For sizes $n = 1-25$, t ranges from seconds to 5 h. Sizes between $n = 30$ and $n = 50$ take from 12 h up to 2 days. Calculations for $n = 55-75$, using a less thorough generation strategy, take from 6 h to 2 days, while the largest $n = 80-100$ runs spend 3−4 days on average.

IV. Evolution of the Properties with Size

In this section, we will discuss the evolution of different properties with cluster size. First of all, we will present our choice of cluster sizes and the most relevant structural features of the lowest-energy isomers. Then, several properties directly related to the geometry of these isomers will be discussed. Subsequently, we will address the energetic properties to be derived from our calculations, including an estimate of specially stable isomer sizes (*magic numbers*). Finally, we will stress how the local properties can be classified according to coordination indices.

A. Structural Properties. Due to the large computational requirements for a global optimization, we have restricted ourselves to the subset of stoichiometric $(AlN)_n$ clusters given by all the isomers from $n = 1$ up to 25 and the isomers with $n = 5k$ ($k \geq 6$ integer) up to $n = 100$. Thus, we have a complete perspective of the smaller sizes plus a sample of the general view among the larger clusters. The lowest-energy isomers found for each of these sizes, together with the symmetry point-groups that they display, are represented in Figure 1. Each isomer is drawn using a different scale, so that the purpose of Figure 1 is mainly to show the structure of the clusters and not to give their actual geometries (these are available upon request to the authors).

To validate these results, we have compared them with those obtained in our previous density functional calculations in small clusters ($n = 1-6$).[2−8] The structures of the lowest-energy isomers found in both calculations are the same, and preliminary results show that they also coincide with the density-functional-derived structures for most of the $n = 7-16$ clusters.[52] The only possible mismatch with the published results lies in the $(AlN)_5$ cluster. While a previous numerical basis-set calculation[4] gives the planar ring of D_{5h} symmetry found here as the lowest-energy isomer, with an AlN-capped cube with C_s symmetry being the second in energy, the situation was reversed when an analytical basis set was used.[8] In both cases, the two isomers were almost degenerate, with their energy differences being 0.39 and 0.06 eV, respectively. The situation is similar in the larger isomers, with the lowest-lying density functional isomer being also the lowest-lying one found here in all but two of them ($n = 8$ and $n = 14$). In these two cases, the second DFT isomer in energy is the one we predict here as the more stable one.

There is, however, a single structural difference worth mentioning. In the $(AlN)_2$ isomer, the density functional calculations predict a strong covalent N−N bond that is not present in our current calculations. This comes as no surprise, given that we have chosen a partially ionic potential model to describe the interactions, with a clearly repulsive overall N−N potential. Nonetheless, neither in the solid state nor in the larger $(AlN)_n$ clusters are these N−N bonds found within the electronic structure results. In fact, the N atoms repel each other more than the Al atoms, since it is usually the N atom that sticks out from the larger structures (e.g., the Al−N−Al angles are smaller than the N−Al−N ones in the small rings and the cylinder-like structures) according to the density functional calculations. This trend is also shown by our lowest-lying isomers (see the insert of Figure 3 below).

Further comparison can be made with the results of Wu et al.[53] These authors employed a particular design model to build the clusters, namely, the restriction of the coordination index (CI) to three, since their main aim was to generate aluminum nitride cages. Even considering this circumstance, the agreement between our lowest-energy isomers and their results is remarkable. The structures with $n \leq 18$ share the same symmetry, with only four exceptions. Even in these cases ($n = 8$, 9, 10, and 18), their lowest-energy configurations coincide with our second-lowest (third in the case of $n = 18$) structures, which lie less than 0.06 E_h above the corresponding lowest-energy ones. Our results, however, differ from theirs for $n > 18$, where our clusters start to display atoms with a CI larger than three. This is reasonable, since our exploration of the potential energy surface is not restricted to this CI = 3 limitation: our aim is to search for the emergence of the bulk behavior (where CI = 4) among the global minimum structures, and the appearance of cagelike clusters can only be an intermediate stage before the appearance of filled, bulklike ones.

A closer view of Figure 1 reveals several clear-cut structural motifs underlying the sequence. Alternate bonds are always preferred over homonuclear bonds, given our potential model (see above). These bonds are arranged as planar ring structures for small clusters ($n = 2-5$): there is a preference for open structures (six- or higher-membered rings) instead of more closed ones (e.g., a cubelike structure for $n = 4$, with six four-membered rings). However, as soon as a 3D structure can be formed with open rings (the two six-membered rings with short bonds for $n = 6$, which are in turn linked by longer bonds), this is preferred over larger rings. This stacking of 6-, 8-, and 10-membered rings is also favored in the $n = 8$, 9, 20, 24, 25, and 30 clusters and is also an important structural element in the $n = 21$ cluster. For $n = 7$, 10−19, 22, 23, and 40 (and also in the other part of the $n = 21$ cluster), the structures are cages formed by six-membered rings, although there are also some four-membered (and a few eight-membered) rings in them: this is expected, since hexagons alone can tessellate a plane but cannot form a regular polyhedron (although the Al_3N_3 hexagons are not regular, the topological limitation still seems to apply).

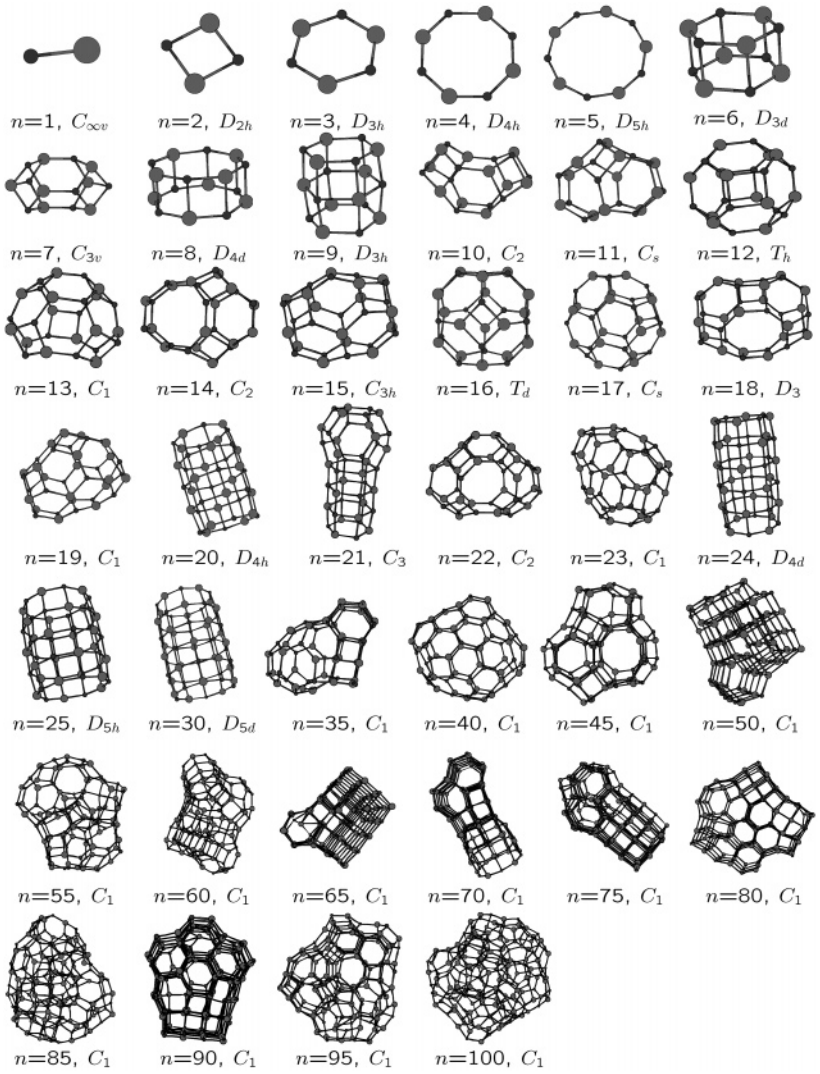

Figure 1. Schematic representation of the structures of the lowest-energy isomers for $(AlN)_n$, $n = 1-100$, with an indication of their point-group symmetry. The large light circles represent Al atoms, and the small dark circles represent N atoms.

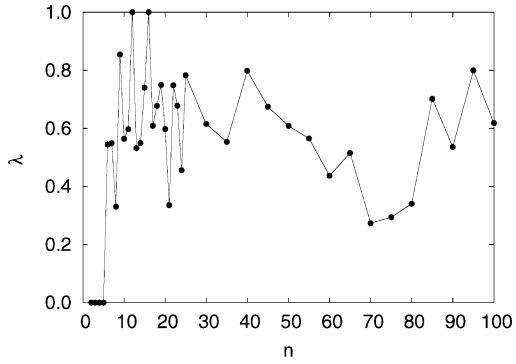

Figure 2. Asymmetry parameter (λ) of the principal inertia moments as a function of the number of AlN units (n) in the cluster.

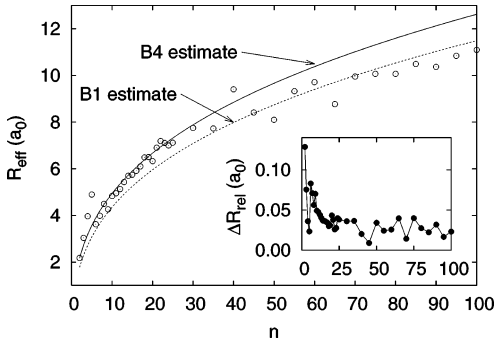

Figure 3. Effective radius for the cluster (R_{eff}, see text) vs the number of units of AlN (n). The insert shows $\Delta R_{rel} = R_{rel}^{N} - R_{rel}^{Al}$, the difference in the average distances to the center of mass, as a function of n.

Clusters with $n = 35$ and $45-100$ show a mixture of elements: some pieces are cagelike, some like stacked rings, and in some cases it seems that cubelike arrangements occur. These cubelike motifs are similar to those in a B1 phase crystal (NaCl-like, with CI = 6 for both atoms), but this phase is only found at high pressures for solid AlN.

There seems to be a competition between two main structural motifs: the square Al_2N_2 and the hexagonal Al_3N_3. These can be identified as prototypical of two different crystalline structures: the square is associated with the B1 phase while the hexagonal motif can be identified with the B4 (or the quite similar B3) phase. AlN occurs in the B4 structure at ambient pressure, although it can also be grown in the B3 phase by epitaxial deposition. It is to be remarked that B4-like structural elements (chairlike six-membered rings in layers, linked by three members to the upper layer and by the other three members to the lower layer) do not abide to a smooth termination, since they tend to leave 2- or even 1-fold coordinated atoms at corners or edges and so they will tend to occur only in the inner part of

even larger clusters. On the other hand, B1-like termination leaves 3-fold coordination even on corners, and thus, it will tend to occur at the borders of the cluster (and in small and medium-sized clusters, where the border takes most of the atoms). Also, it is worth mentioning that, in some of the clusters presenting six-membered Al_3N_3 rings, their stacking is correct. However, since there is no periodic-like hexagonal layer to allow for the completion of the tetrahedral coordination, all six members of the ring tend to link to the rings above and below it, instead of just three members to each of them as in the B4 structure. Thus, the faces of these stackings present Al_2N_2 four-membered rings. Nevertheless, as we shall see below, these B1-like features are less important than the simple view the structures may suggest. In fact, a comparison with the lowest-energy isomers of $(NaCl)_n$ (with a B1 solid structure) obtained by Phillips et al.,[50] shows that the coincidences with our $(AlN)_n$ clusters up to $n = 14$ ($n = 2$, 3, 6, 7, and 9) are precisely in the cases where the $(NaCl)_n$ cluster displays more B4-like features. This is in contrast with the cubic arrangements displayed by all other $(NaCl)_n$ lowest-energy isomers.

There also seems to be a preference for planar-like structures in our calculations. This may be linked to the fact that we have neglected polarization effects (average point-charge electric field module over the atoms is about 0.06 E_h/ea_0 for $n > 25$).

The symmetry of the lowest-energy isomers is linked to their structural types. In this way, the rings and stacked rings display a high-order axis, while the cages present a lower symmetry except for some particular sizes (most notably, the tetrahedral $n = 12$ and 16 and the 3-fold axis for $n = 7$, 15, 18, and the cagelike part in $n = 21$). However, the mixture of different elements present in the larger clusters deprives them of symmetry: all of the clusters with $n \geq 35$ are asymmetric (C_1).

B. Geometry-Related Properties. While the precise geometry of small molecules and crystalline phases is usually one of the key properties in their understanding, the geometry of clusters and aggregates with a large number of atoms involves so many variables that a raw discussion of it is out of question. Thus, averages and other statistical measures and also geometry-related properties are typically used to characterize the geometry of these materials.

A good geometrical indicator of the shape of a cluster is the asymmetry parameter of its principal inertia moments, $\lambda = (I_a + I_b - I_c)/I_c$ (ordered as $I_a \leq I_b \leq I_c$). If $\lambda = 0$, the cluster is planar (linear if I_a is also zero), while its value goes to 1 for spherical tops ($I_a = I_b = I_c$). Spherical-like clusters would have large λ values, while planar-like or quasi-linear clusters would have small λ values. Figure 2 shows the evolution of this property with the size of the cluster for the lowest-energy isomers. It is easy to locate the planar clusters ($n = 2-5$) and the tetrahedrally symmetric ones ($n = 12$ and 16, those with $\lambda = 1$). The clusters with $n = 8$ (oblate, plane-like) and $n = 21$ and 24 (prolate, linear-like) also stand out from below. No clear trend can be established beyond that, specially for the larger clusters, although it seems that those with larger λ values ($n =$ 40, 85, and 95) display indeed a more spherical shape.

The inertia moments can also be used to define an effective radius for the cluster, by taking the average inertia momentum as defining a solid sphere equivalent to the cluster, $2/5MR_{eff}^2 = 1/3(I_a + I_b + I_c)$. This R_{eff} is depicted in Figure 3, together with estimates for the effective radii of spherical portions of the B1 and B4 phases. These estimates are taken by assuming that the density of atoms in the sphere is that in the corresponding solid (as optimized using the current potential model). We have further corrected this radius by subtracting half the interatomic distance in the corresponding solid, to account for the different sphere definitions (according to nuclear positions in the inertia momentum and according to atomic volumes and radii in the solid phase estimates). It seems that the cagelike clusters adhere better to the B4 estimate, while the larger clusters appear as more B1-like. However, this has to be taken as a crude estimate, greatly influenced by the shape of the cluster.

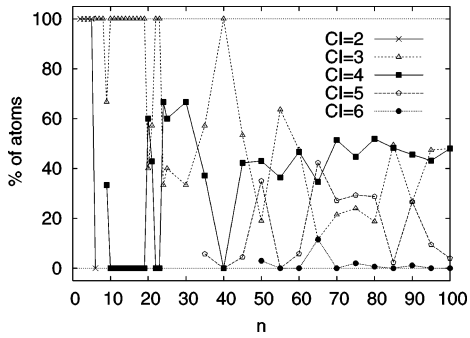

Figure 4. Percentage of atoms with a given coordination index (CI) vs the number of units of AlN (n).

The insert of Figure 3 shows the difference in the average distances relative to the center of mass of N and Al atoms ($\Delta R_{rel} = R_{rel}^N - R_{rel}^{Al}$). There is a small but unequivocal trend for N atoms to be further from the center of mass than Al atoms. This is not just because the larger Al mass tends to push the center of mass toward Al atoms, since it is also present in the high-symmetry clusters. As mentioned above, this is also shown by the density functional calculations. In terms of the potential model, it is related to the values of the N−N repulsion, slightly larger than those of the Al−Al repulsion at the next-nearest-neighbor distances (0.1 eV vs 0.05 eV, respectively).

A key property in the identification of the emergence of bulklike properties within a cluster is the coordination index, CI. Although more refined definitions in terms of the electronic structure can be given,[3,6,8,35] for the present atomistic simulations, a distance criterion for the heteronuclear bonds suffices: an Al−N pair is considered to be bonded whenever its distance is smaller than 3.8 a_0 (2.01 Å). Homonuclear bonds are not considered, since both the N−N and the Al−Al bonds have been shown to be unfavored for all but the smallest stoichiometric clusters. The percentage of atoms displaying a given CI for the lowest-energy isomers of each size (n) is then depicted in Figure 4. The dominance of each of the structural motifs identified in subsection 4.1 is clearly seen in this graph. The smaller isomers were planar rings, where all atoms display CI = 2; no other isomer displays this CI, nor CI = 1 (the AlN molecule has been omitted). The cagelike structures ($n = 6-8$, 10−19, 22, 23, and 40) only have tricoordinated atoms (CI = 3). Ring-stacking structures display tetracoordinated atoms (CI = 4), but the coordination is quasi-planar, not tetrahedral as in the solid. The hybrid structures of the largest clusters ($n \geq 35$, except for $n = 40$ and 55) display some pentacoordinated atoms (CI = 5), and the $n = 50$, 65, 75, 80, and 90 display a small number of hexacoordinated atoms. A careful examination shows that these clusters display some B1-like portions in their structure (together with the $n = 70$ isomer, but in this case, all of the atoms in this B1-like part belong to the surface).

The above data leads to the following global image, already hinted in the previous subsection: there is a competition between the B4-like and B1-like structural motifs. In the periodic solid, the B4 structure is only 3.7 μE_h (0.1 eV) below the B1 structure. This small difference can be easily overturned by the ease of low-energy termination in the B1-like motifs, as compared with

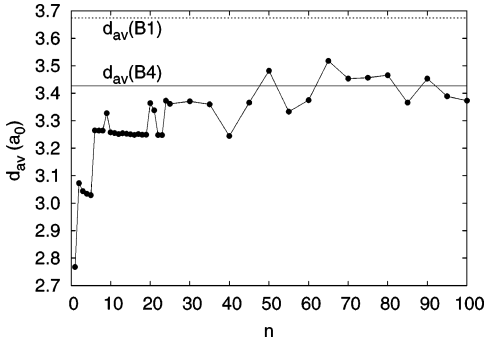

Figure 5. Average first-neighbor distance (d_{av}) vs the number of AlN units (n). The solid line displays the average value for the B4 crystal, the dotted line the nearest-neighbor distance in the B1 crystal.

the B4-like: in order to avoid high-energy 1- or 2-fold coordinated atoms, a B4-like motif has to be enclosed within a 3-fold coordinated cage, which in turn must adapt to the tetrahedral-like structure in order to avoid dangling or too-stretched bonds. This is apparent in the more B4-like isomers, those with $n = 85$, 95, and 100 (among the largest), where 5-fold coordination is quite small and 6-fold coordination is absent. The tetrahedral coordination appears in these isomers, but almost 50% of the atoms display 3-fold coordination, that is, the surface of the cluster still contains more atoms than its interior. Thus, surface effects are still very important even for the largest clusters presented here.

Finally, we show the evolution of the average nearest-neighbor distance (d_{av}) with the cluster size in Figure 5. The average nearest-neighbor distances of the B1 and B4 phases optimized using the same potential model (3.674 and 3.427 a_0, respectively) are shown in order to help the comparison. Again, the different structural motifs are apparent in this trend. The AlN molecule stands below the rest, with the ring structures coming next. Cage structures display a fairly constant nearest-neighbor distance, 3.244−3.265 a_0, while ring stackings present slightly different average nearest-neighbor distances depending on the border-to-inner part of the stacking ratio. The larger, hybrid clusters present a more variable average distance. The more B1-like clusters ($n = 50$, 65−80, and 90) have d_{av} larger than the B4 structure, while the more B4-like present distances slightly smaller. In any case, none of these large clusters ($n > 40$) d_{av} is further than 0.1 a_0 from the B4 value. This is striking, since it seems that, although B1-like coordinations develop in order to achieve a low-energy termination of the cluster, their weight in the global structure (as given by the average distance) is compensated by the lower coordination atoms. A further discussion of the connection between average distances and coordinations is left for subsection 4.4.

C. Energetic Properties. The main energetic output in an atomistic pair potential calculation is the binding energy, the energy of the given atomic configuration with respect to a reference free-atom limit. In our case, the binding energy for an $(AlN)_n$ cluster is computed as

$$E_n = \sum_{i=1}^{n}\sum_{j=1}^{n} V_{AlN}(r_{AliNj}) + \sum_{i=1}^{n-1}\sum_{j=i+1}^{n} (V_{AlAl}(r_{Al_iAl_j}) + V_{NN}(r_{N_iN_j})) \quad (2)$$

and the reference is the +2/−2 ai PI ionic states used in the generation of the potentials. Table 2 collects these binding energies for the lowest-energy isomers of each size. It is of course evident that this quantity must decrease more or less proportionally to the number of AlN units in the cluster, so that in the $n \rightarrow \infty$ limit it becomes an extensive quantity, that is, E_n/n becomes independent of n (and equivalent to the crystalline limit). To provide both (i) numerical values of this limit and (ii) a better grasp of the stabilization involved in the formation of these clusters, we also include in Table 2 the relative binding energy with respect to the monomer, $E_n^r = E_n/n - E_1$. This is the average energy with which an AlN pair is bound within the cluster of size n, and its absolute value tends to increase with n. This effect is related to the increase of bulklike character of the average cluster atoms when the size increases: the percentage of surface (strained, low-coordinated) atoms decreases when the size increases and three-dimensional bond networks develop, being negligible for the macroscopic size limit. The trend in E_n^r is indeed a decreasing one, although some exceptions appear when the main structural motifs change from one cluster to the next. Especially puzzling is the fact that the B1-like dominated isomers ($n = 50$, 65−80, 90) seem to bind the AlN units slightly more, on average, than the B4-like dominated ones ($n = 85$, 95, 100) among the largest clusters.

TABLE 2: Total Binding Energy (E_n) and Relative Binding Energy with Respect to the Monomer ($E_n^r = E_n/n - E_1$) for the Lowest-Energy Isomer Found among $(AlN)_n$ Clusters of Size n

n	E_n[a]	E_n^r	n	E_n	E_n^r
1	−1.2061	0.0000	21	−33.6713	−0.3973
2	−2.8596	−0.2237	22	−35.2884	−0.3979
3	−4.4972	−0.2930	23	−36.9203	−0.3992
4	−6.0952	−0.3177	24	−38.5830	−0.4016
5	−7.6776	−0.3294	25	−40.2063	−0.4022
6	−9.3516	−0.3525	30	−48.3446	−0.4054
7	−10.9048	−0.3517	35	−56.3109	−0.4028
8	−12.5765	−0.3660	40	−64.4969	−0.4063
9	−14.2175	−0.3736	45	−72.5515	−0.4062
10	−15.7932	−0.3732	50	−80.7229	−0.4084
11	−17.4308	−0.3786	55	−88.6308	−0.4054
12	−19.1181	−0.3871	60	−96.8161	−0.4075
13	−20.6593	−0.3831	65	−105.2197	−0.4127
14	−22.3057	−0.3872	70	−113.2638	−0.4120
15	−23.9591	−0.3912	75	−121.3749	−0.4123
16	−25.5901	−0.3933	80	−129.5345	−0.4131
17	−27.1570	−0.3914	85	−137.2240	−0.4083
18	−28.8186	−0.3950	90	−145.8404	−0.4144
19	−30.4315	−0.3956	95	−153.5824	−0.4106
20	−32.0824	−0.3981	100	−161.6977	−0.4109

[a] Energies in hartrees.

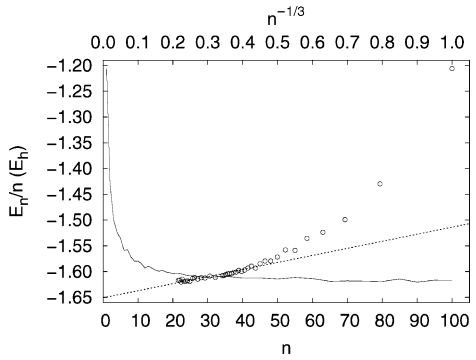

Figure 6. Binding energy per molecule (E_n/n) for $(AlN)_n$ clusters. The solid line is to be read in the lower x axis (n, number of AlN units), while the open circles are to be read in the upper axis ($n^{-1/3}$). The dotted line corresponds to a E_n/n vs $n^{-1/3}$ linear fit excluding the $n \leq 8$ values.

We have plotted in Figure 6 the binding energies per molecule, E_n/n, vs the number of AlN units in the cluster. As previously stated, this property (differing by a constant from

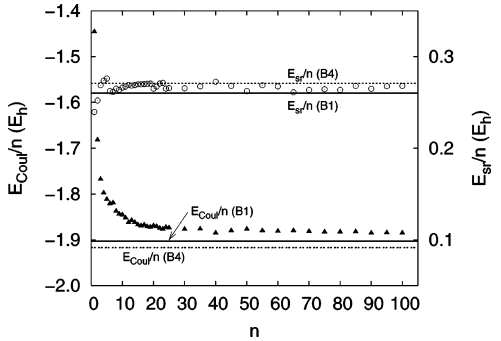

Figure 7. Coulombic energy per molecule (E_{Coul}/n, filled triangles to be read in the left axis) and short-range energy per molecule (E_{sr}/n, empty circles to be read in the right axis) for $(AlN)_n$, $n = 1-100$ clusters. Notice that the right axis is expanded to a 2:1 ratio compared with the left axis.

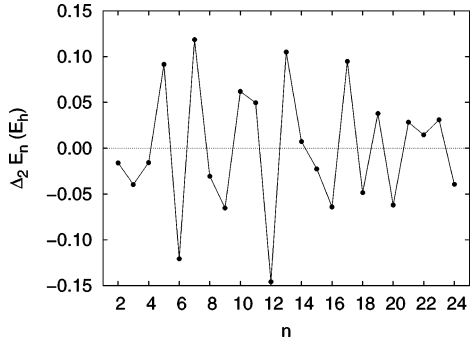

Figure 8. Second energy difference ($\Delta_2E_n = 2E_n - E_{n-1} - E_{n+1}$) for the $n = 2-24$ lowest-energy $(AlN)_n$ clusters.

E_n^r in Table 2) decreases to an asymptotic value as the cluster size increases. The rate of this decrease can be modeled in different manners: we have chosen a $a + b/n^{1/3}$ functional form, which assumes that the evolution is related to the truncation of the $1/r$ Coulombic interaction at the cluster border when compared with the crystal. We find a quite good fit, where $a = -1.6508 \pm 0.0025$ E_h and $b = 0.137 \pm 0.007$ E_h when eliminating the $n \leq 8$ clusters from the fit to avoid the exaggerated surface effects of these small clusters. The asymptotic limit of this expression, a, is to be compared with the corresponding bulk crystal values of the B4 and B1 phases computed using the same potential model, namely, -1.6465 and -1.6428 E_h for the B4 and B1 phases, respectively. Although both of them lie above the asymptotic limit, even considering the error bar, the B1 phase value is twice further from a than the B4 one.

In our model, the total energy is obtained as a sum of two contributions (see eq 1): the purely electrostatic Coulombic contribution (E_{Coul}), which is a long-range term that decreases as $1/r$, and another one that models all the nonclassical energetic contributions, which we label as short-range energy (E_{sr}) due to its much faster decrease with increasing distance. The evolution of both contributions with the cluster size is shown separately in Figure 7. It is readily seen that the short-range term stabilizes for cluster sizes much smaller than the Coulombic term (notice also that the scale is twice as large). This is, of course, linked to the cluster size and the range of each interaction: the short-range interaction is mostly restricted to first- and perhaps second-neighbors, while the Coulombic interaction decays more slowly, with the surface contribution being nonnegligible even for atoms in the inner part of the cluster. We have also included the corresponding values for the B4 and B1 crystals, for the sake of comparison. In the short-range case, the small separation between them is on the order of the oscillations in the cluster values, and in fact it is seen that B4-like clusters appear closer to the corresponding B4 bulk short-range energy and B1-like clusters closer to the B1 bulk value. However, the Coulombic terms for the clusters are still clearly above both B1 and B4 bulk values, an indication of the slow convergence of the point-charge interactions known as the Madelung problem.

To test the relative stability of the clusters of different sizes, it is customary to compute the second energy difference $\Delta_2E_n = 2E_n - E_{n-1} - E_{n+1}$. Sizes with negative Δ_2E_n values are thus stable on average with respect to the gain and the loss of an AlN molecule, and those with specially low values are expected to be the most observed in mass spectra (assuming long times of flight and small energy barriers). We have computed this differences in the available range, $n = 2-24$, and depicted them in Figure 8. It appears that clusters with sizes $n = 12$ and 6 are specially stable and to a lesser extent those with $n = 9$, 16, 20, and 18. Clusters with $n = 3$, 24, 8, 15, 2, and 4 are also stable using this criterion (the sizes are listed in decreasing stability order) but less than the previous ones. It is remarkable that all of the above-mentioned stable isomers display high-order symmetries, with $n = 18$ being the lowest-order one (D_3, an order 6 group) among them. This is well-known in general, since high-symmetry clusters tend to display regular arrays with no low-coordination atoms and few angular strains, thus resulting in specially stable structures. This is indeed the case of the two tetrahedrally symmetric structures, the most stable one ($n = 12$, a vertex-truncated cube) and the fourth in stability ($n = 16$, an edge-truncated cube). The fact that the latter is not at the top of the list is probably related to the fact that the loss of an AlN molecule leads it into another symmetric structure, $n = 15$, which in turn is less stable than it should be because the gain of AlN leads it back to the $n = 16$ structure. The $n = 6$ size is especially stable because it marks the onset of 3-D structures after the planar ones, while $n = 9$ is the first one displaying a coordination index of 4 (i.e., with atoms in face-like positions instead of in edge-like positions within the cluster structure).

D. Influence of the Atomic Coordination on the Cluster Properties. We have seen in the previous subsections how the global and average properties of these clusters show different trends according to the structural motifs present on each of them. These trends are mixed together within the global properties, being only apparent when a single structural motif dominates (e.g., the cages for $n = 6-19$). However, they should be clearly displayed in the local properties within each of the motifs, although that puts forward the problem of clearly distinguishing which atoms belong to which motif. A compromise can be reached if we classify the atoms according to their CI. In this way, we can assign an average local property to a group of atoms within a given cluster and then study how these properties relate among different clusters.

This is done with the average first-neighbor distance in Figure 9. The data points for each kind of atom (Al, N) and each coordination (CI = 2, 3, 4, 5, and 6) share the same abscissa, different data points in the same abscissa correspond to clusters of different sizes. The average distances of the two solid phases are also included. It is apparent, within a given CI, that the differences in the nearest-neighbor distances for Al and N atoms are minimal, while the distances increase when considering increasing CI. The dispersion among the data points within a given CI is smaller than the separation between different CIs, and so we can conclude that the interatomic distance is clearly dominated by the coordination and not by the cluster size. Also,

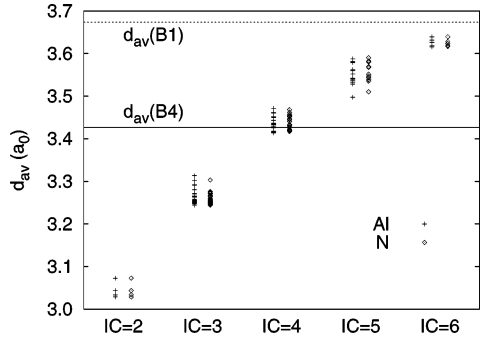

Figure 9. Average first-neighbor distance (d_{av}) of Al and N atoms vs their coordination index. The average distances in the B4 (CI = 4) and B1 (CI = 6) crystals are also included.

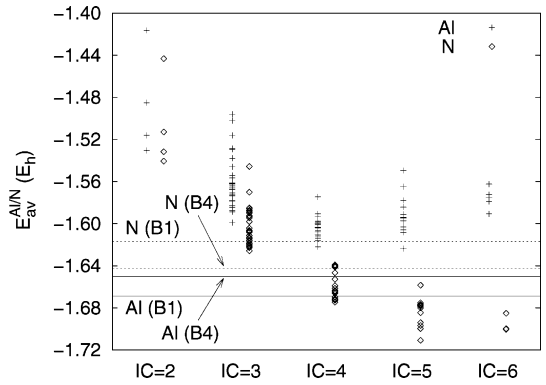

Figure 10. Average interaction energy (E_{av}^{i}) of Al and N atoms vs their coordination index. The corresponding values for the B4 (CI = 4) and B1 (CI = 6) crystals are also included.

the CI = 4 distances are quite close to the B4 value, even though they correspond to square-planar-like configurations in some cases (which makes them slightly larger than those of tetrahedral configurations). On the other hand, the CI = 6 distances are still below the average B1 value, perhaps indicating that the B1 bulklike atoms are still the absent form in these clusters and that sizes greater than $n = 100$ are necessary to achieve the d_{av} B1 limit.

The same analysis has been performed with the average interaction energy of a given atom with the rest of atoms of the cluster, presented in Figure 10. The different energies for the N and Al atoms in the B4 and B1 phases are also included. The dispersion in these energies is larger than that in the distances, and the data points within a given CI expand an energy range that overlaps with those corresponding to other CIs. However, clear trends can still be detected. The trends for Al and N atoms differ, which is only partially surprising: while most of the first-neighbor contributions should be equal, as shown by the average distance trends, the long-range contributions differ. As previously stated, N atoms tend to position slightly further from the middle of the cluster than the Al atoms, due to the stronger second-neighbor repulsions. This has an effect over the global long-range contributions that lowers the N average interactions with respect to the Al ones. In this way, the N atoms appear to increase their stabilization when increasing the coordination, although this trend seems to stop around CI = 6, with an average interaction energy on the same range as the CI = 5 case. However, the Al atoms present a clear minimum of interaction energy at CI = 4, with a smaller stabilization for CI = 5 and CI = 6.

It is surprising that the stabilization trends displayed by the cluster atoms are opposite to those for the bulk solids: Al is always below N in the solids, the B1 (CI = 6) N being above the B4 (CI = 4) N and the B1 Al below the B4 Al. This apparent contradiction has a simple explanation. Due to their high symmetry, the Al and N positions are interchangeable in both the B1 and B4 crystal phases and thus the electrostatic stabilization on a given phase is equal for Al and N. Since the second-nearest-neighbor distances are also the same, the stronger N−N repulsion makes this atom higher in energy than Al in both solids. Furthermore, the split is larger for the B1 phase than for the B4, owing to the larger number of second-nearest-neighbor interactions in this structure; since both phases were quite close in energy, this accounts for the energy ordering of the bulk atoms. Comparing these values with the cluster trends, it is seen that all of the cluster atoms are still far away from the solid behavior, even those with bulklike coordinations. As hinted in the previous paragraph, this is due to the unconverged long-range electrostatic interactions: the Al and N distributions are still different (see the insert of Figure 3), and even this slight bias toward the surface for N atoms creates a clear distinction in the energy trends that is in some senses opposite to what should be expected of bulklike systems.

V. Conclusions

In this work, global optimizations of stoichiometric $(AlN)_n$ clusters with sizes $n = 1-25$, 30, 35,..., 95, 100 have been conducted employing a pair potential energy model and the BH method for the potential energy surface search. The results are in agreement with those obtained in previous electronic structure calculations for the smaller sizes ($n = 1-6$) and optimizations restricted to cagelike clusters (see ref 53). Thus, they can be employed as input for a further study employing electronic structure methods.

Structure-wise, there are three well-differentiated regimes. Small clusters ($n = 2-5$) present 2-fold coordination and planar ring structures. Medium-sized clusters ($n = 6-40$) have two competing structural types: stacked rings ($n = 6$, 8, 9, 20, 24, 25, and 30) and cages mainly formed by hexagonal rings ($n = 7$, 10−19, 22, 23, and 40). Clusters with $n = 21$ and 35 advance the main structural features of the large clusters ($n = 45-100$): a mixture of stacked rings and cagelike features, in some cases having a clear set of atoms in the interior part of the cluster (i.e., not on its surface). These structural motifs lead to configurations similar to those in the AlN solid (B4 phase, tetrahedral coordination) but also similar to those in a more ionic solid like NaCl (B1 phase, octahedral coordination). While the B4 phase is preferred in the bulk, the B1 phase has a smoother termination which leaves no low-coordinated atoms and, thus, its features may be preferred for clusters with large surface effects. Therefore, a competition exists that makes some of the large clusters more B4-like ($n = 45$, 55, 60, 85, 95, 100) and some others more B1-like ($n = 50$, 65−80, 90).

The geometry-related properties are clearly dominated by the above-mentioned structural motifs, showing distinct trends for each of them. However, even though the B1-like isomers indeed display atoms with coordination indices of 5 (B1 face) and 6 (B1 interior), the average nearest-neighbor distance in the large isomers ($n > 40$) is within 0.1 a_0 (0.05 Å) of the B4 phase average value. Regarding the energetic properties, it is seen that the convergence rate to the bulk binding energy is quite slow. Nonetheless, an extrapolation assuming that the size effects are dominated by the Coulombic terms is possible and leads to a value close to that of the B4 phase. The Coulombic dominance in the surface effects is explicitly proven, while showing that the short-range terms do converge to a narrow band between the B4 and B1 values (the oscillations being related to the B1-

like and B4-like character of the clusters). The relative stability of the isomers shows that $n = 12$ and 6, and to a lesser extent, 9, 16, 20, and 18 clusters are especially stable and more likely to occur in long time-of-flight mass spectra experiments. They do display a quite high symmetry, as is common in the so-called *magic number* clusters.

Finally, we have computed average local geometries and energies as a function of the CI. These results show that convergence to the bulk values can be locally achieved as soon as the cluster has an interior region. However, surface effects can stabilize structures with different coordinations than the B4 phase tetrahedra (like the B1-like octahedra). This is displayed by some of our results, with corresponding deviations from the bulklike B4 behavior.

Acknowledgment. This research has been funded by the Spanish Ministerio de Educación y Ciencia, Grant BQU2003-06553. A.C. wishes to thank the Spanish Ministerio de Educación y Ciencia for her Ramón y Cajal position.

References and Notes

(1) Martin, T. P. *Phys. Rep.* **1983**, *95*, 167−199.
(2) Kandalam, A. K.; Pandey, R.; Blanco, M. A.; Costales, A.; Recio, J. M.; Newsam, J. M. *J. Phys. Chem. B* **2000**, *104*, 4361−7.
(3) Costales, A.; Kandalam, A. K.; Martín Pendás, A.; Blanco, M. A.; Recio, J. M.; Pandey, R. *J. Phys. Chem. B* **2000**, *104*, 4368−74.
(4) Kandalam, A. K.; Blanco, M. A.; Pandey, R. *J. Phys. Chem. B* **2001**, *105*, 6080−4.
(5) Kandalam, A. K.; Blanco, M. A.; Pandey, R. *J. Phys. Chem. B* **2002**, *106*, 1945−53.
(6) Costales, A.; Blanco, M. A.; Martín Pendás, A.; Kandalam, A. K.; Pandey, R. *J. Am. Chem. Soc.* **2002**, *124*, 4116−4123.
(7) Costales, A.; Pandey, R. *J. Phys. Chem. A* **2003**, *107*, 191−197.
(8) Costales, A.; Kandalam, A. K.; Pandey, R. *J. Phys. Chem. B* **2003**, *107*, 4508−4514.
(9) Nakamura, S. In *Proceedings of International Symposium on Blue Laser and Light Emitting Diodes*; Yoshikawa, A., Kishino, K., Kobayashi, M., Yasuda, T., Eds.; Chiba University Press: Nishi-Chiba, Japan, 1996; p 119.
(10) Nakamura, S.; Fasol, G. *The blue laser diode;* Springer-Verlag: Berlin, Germany, 1997.
(11) Fassol, G. *Science* **1997**, *278*, 1902.
(12) Morkoæ, H.; Mohammad, S. N. *Science* **1995**, *267*, 51.
(13) Ponce, F. A.; Bour, D. P. *Nature* **1997**, *386*, 353.
(14) Belyanin, A. F.; Bouilov, L. L.; Zhirnov, V. V.; Kamenev, A. I.; Kovalskij, K. A.; Spitsyn, B. V. *Diamond Relat. Mater.* **1999**, *8*, 369.
(15) Timoshkin, A. Y.; Bettinger, H. F.; Schaefer, H. F. *J. Am. Chem. Soc.* **1997**, *119*, 5668.
(16) Lei, T.; Fanciulli, M.; Molnar, R. J.; Moustakas, T. D. *Appl. Phys. Lett.* **1991**, *59*, 944.
(17) Edgar, J. H. *J. Matter Res.* **1992**, *7*, 235.
(18) Wales, D. J.; Doye, J. P. K. *J. Phys. Chem. A* **1997**, *101*, 5111.
(19) Xiang, Y.; Jiang, H.; Cai, W.; Shao, X. *J. Phys. Chem. A* **2004**, *108*, 3586−3592.
(20) Shao, X.; Xiang, Y.; Cai, W. *Chem. Phys.* **2004**, *305*, 69−75.
(21) Shao, X.; Cheng, L.; Cai, W. *J. Comput. Chem.* **2004**, *25*, 1693−1698.
(22) Xiang, Y.; Cheng, L.; Cai, W.; Shao, X. *J. Phys. Chem. A* **2004**, *108*, 9516−9520.
(23) Doye, J. P. K.; Wales, D. J.; Miller, M. A. *J. Chem. Phys.* **1998**, *15*, 8143−8153.
(24) Calvo, F.; Doye, J. P. K.; Wales, D. J. *J. Chem. Phys.* **2001**, *114*, 7312−7329.
(25) Doye, J. P. K.; Hendy, S. C. *Eur. Phys. J. D* **2003**, *22*, 99−107.
(26) Doye, J. P. K. *J. Chem. Phys.* **2003**, *119*, 1136−1147.
(27) Doye, J. P. K. *Phys. Rev. B* **2003**, *68*, 195418.
(28) Doye, J. P. K.; Wales, D. J. *Chem. Phys. Lett.* **1996**, *262*, 167−174.
(29) Doye, J. P. K.; Wales, D. J.; Branz, W.; Calvo, F. *Phys. Rev. B* **2001**, *69*, 235409.
(30) Yoo, S.; Zeng, X. C. *Angew. Chem., Int. Ed.* **2005**, *44*, 1491.
(31) Yoo, S.; Zhao, J. J.; Wang, J. L.; Zeng, X. C. *J. Am. Chem. Soc.* **2004**, *126*, 13845.
(32) Yoo, S.; Zeng, X. C.; Zhu, X.; Bai, J. *J. Am. Chem. Soc.* **2003**, *125*, 13318.
(33) Doye, J. P. K.; Wales, D. J. *Phys. Rev. B* **1999**, *59*, 2292−2300.
(34) Doye, J. P. K.; Meyer, L. 2005.
(35) Bader, R. F. W. *Atoms in Molecules*; Oxford University Press: Oxford, U.K., 1990.
(36) Xu, Y.-N.; Ching, W. Y. *Phys. Rev. B* **1993**, *48*, 4335−4351.
(37) Blanco, M. A.; A. Martín Pendás.; Luaña, V. *Comput. Phys. Commun.* **1997**, *103*, 187−302.
(38) Recio, J. M.; Francisco, E.; Flórez, M.; Martín Pendás, A. *J. Phys.: Condens. Matter* **1993**, *5*, 4975−4988.
(39) Blanco, M. A.; Recio, J. M.; Francisco, E.; Costales, A.; Luaña, V.; Martín Pendás, A. *Radiat. Eff. Defects Solids* **1999**, *151*, 223−228.
(40) Gordon, R. G.; Kim, Y. S. *J. Chem. Phys.* **1972**, *56*, 3122.
(41) Kim, Y. S.; Gordon, R. G. *Phys. Rev. B* **1974**, *9*, 3548.
(42) Kim, Y. S.; Gordon, R. G. *J. Chem. Phys.* **1974**, *60*, 4332.
(43) Cohen, A. J.; Gordon, R. G. *Phys. Rev. B* **1975**, *12*.
(44) Francisco, E. *The cluster program*; Universidad de Oviedo: Oviedo, Spain, 2001−2005.
(45) Wales, D. J. *Energy Landscapes: Applications to Clusters, Biomolecules and Glasses*; Cambridge University Press: Cambridge, U.K., 2004.
(46) Wales, D. J.; Scheraga, H. *Science* **1999**, *285*, 1368.
(47) White, R. P.; Mayne, H. R. *Chem. Phys. Lett.* **1998**, *289*, 463.
(48) Yoo, S.; Zeng, X. C. *J. Chem. Phys.* **2003**, *119*, 1442.
(49) Liu, D.; Nocedal, J. *Math. Prog B* **1989**, *45*, 503−528.
(50) Phillips, N. G.; Conover, C. W. S.; Bloomfield, L. A. *J. Chem. Phys.* **1991**, *94*, 4980−4987.
(51) Bonchev, D.; Rouvray, D. *Chemical Graph Theory: Introduction and Fundamentals*; Abacus Press: New York, 1991.
(52) Costales, A.; Blanco, M. A.; Francisco, E.; Pandey, R. *J. Phys. Chem. B* **2005**.
(53) Wu, H.; Zhang, F.; Xu, Z.; Zhang, X.; Jiao, H. *J. Phys. Chem. A* **2003**, *107*, 204−209.